78

Electron Current Collection by a Positively Charged Tether Using a Particle-In-Cell Method

by

Tatsuo Onishi

Submitted to the Department of Aeronautics and Astronautics
in partial fulfillment of the requirements for the degree of

Master of Science in Aeronautics and Astronautics

at the

MASSACHUSETTS INSTITUTE OF TECHNOLOGY

May 1998

Author .....
Department of Aeronautics and Astronautics
May 18, 1998

Certified by .....
Manuel Martinez-Sanchez
Professor
Thesis Supervisor

Accepted by .....
Jaime Peraire
Chairman, Department Graduate Committee

Electron Current Collection by a Positively Charged Tether Using a Particle-In-Cell Method

by

Tatsuo Onishi

Submitted to the Department of Aeronautics and Astronautics
on May 18, 1998, in partial fulfillment of the
requirements for the degree of
Master of Science in Aeronautics and Astronautics

Abstract

A Particle-In-Cell (PIC) method is developed and applied to simulate the electron current collection by a positively charged tether in a quiescent unmagnetized plasma under the Maxwellian collisionless condition. We compare our result with the exact solution to validate our code. This simulation is performed with the help of a non-rectangular grid and a new treatment of the outside boundary condition. The error induced by a non-rectangular grid is calculated and the effect of it is considered. The outside boundary treatment improves the accuracy of the amount of current collected by the tether. A very small ion mass is used and it is verified to speed up the computation considerably without loss of quality in the result. The comparison with the exact solution shows that our code provides good qualitative and quantitative approximations.

Thesis Supervisor: Manuel Martinez-Sanchez
Title: Professor

Acknowledgments

I would like to show my profound appreciation to Professor Manuel Martinez-Sanchez for the chance he gave me to work on this splendid project. He always lighted up the path I was walking and led me to the right place. And I would also like to send my eternal thanks to my parents, Tadao and Yoshiko Onishi, who always back me up to walk the path.

Contents

List of Figures

List of Tables

Chapter 1

Introduction

In tethered satellite technology, it is important to estimate how many electrons a spacecraft can collect from its surrounding plasma by its positively charged tether. The analysis is, however, very difficult because of the small but significant Geomagnetic field and the spacecraft's relative motion to both ions and electrons [5]. One of the approaches for the solution to this problem is the numerical method. In the numerical analysis of space plasma, one of the most reliable methods has been the Particle-In-Cell (PIC) method. In this thesis, we develop a PIC code for a two dimensional collisionless plasma without magnetic field.

The original Particle-In-Cell code was established by *Birdsall* at U.C.Berkeley. [1] Using a rectangular grid and finite-size particles, he has studied the effects of grid size and timestep on the simulation and relevant numerical instabilities. As the "bible" to PIC users, his publications give us excellent criteria for its numerical stability and reliability. The concept of PIC in our code is mostly from this "bible".

The usage of a rectangular grid and a finite-size particle, however, poses some problems. In the usual numerical application, very complicated configurations require non-rectangular body fitted grids. Being defined by the grid size, the finite-size particle can not maintain its constant size any more. In this thesis, we estimate the error induced by the use of a non-rectangular grid and consider the effect on our simulation.

In order to validate our code, we apply it to the current collection by a cylindrical

tether in a collisionless unmagnetized plasma, near the boundary of Orbital Motion Limited (OML) regime, for which an exact solution exists [4]. The OML theory, which will be further discussed in the next chapter, applies in the limit of large ratios of Debye length to radius.

In the vicinity of the tether, there is a region called "sheath", where quasi-neutrality does not apply. That is to say, the densities of ions and electrons differ from each other considerably. In order to reproduce this region, we follow the motion of both ion and electron particles. Since the mass ratio of an ion to an electron is very large, we would need a great number of iterations till both species come to have converged distributions, without having electrons travel a large distance in one iteration, which would induce a large error in the energy conservation. However, the fact that, at tether potentials much greater than the ion temperature, we can assume that no ion is absorbed by the tether, solves this problem of the computational cost. In theory, the ion density at an arbitrary point does not depend on its mass when its distribution is Maxwellian.

Since some electrons are absorbed on the surface of the tether, there is also a region called "pre-sheath" outside the sheath, where quasi-neutrality prevails but the electric potential is not the same as that of the ambient plasma at infinity.

In a computation, we have to use a finite region to calculate field quantities. And, because of the limited memory on a computer, we can not use an infinitely large grid to include the pre-sheath region. Therefore we have to clip a computational region out of this infinitely large space, and determine the outer boundary conditions by considering only the quasi-neutrality and the collisionless nature of the plasma. The limitation of the number of particles available in a computer gives fluctuating local boundary conditions. To avoid this, we use a spatially averaged boundary condition.

The goal of this thesis is to establish a code to simulate a collisionless unmagnetized plasma in and near the sheath region. Based on this code, we plan to include later all the phenomena encountered by a tethered satellite, such as Geomagnetic field and plasma cross-flow.

Chapter 2

Orbital Motion Limit (OML) Current

Current collection by spherical and cylindrical probes (tethers) was first analyzed by *Lagmuir* and *Mott-Smith* [6] , who named the thin cylinder limit, 'Orbital Motion Limit (OML)'. When OML theory applies, namely, when the ratio of the probe (tether) radius to the Debye length of the plasma is so small that the shielding becomes unimportant, the number of electrons absorbed by the probe is determined from energy and angular momentum considerations alone.

The OML limit can be described in terms of the effective potential. [3] Let J and E be the angular momentum and the energy of a particle, respectively. From the energy conservation and the angular momentum conservation of an electron in two dimensions, although the velocity $v_{||}$ along the cylinder axis can be nonzero, we have

$$E = \frac{1}{2} m_e \left(v_r^2 + v_\theta^2 \right) + q\phi \tag{2.1}$$

$$J = m_e r v_\theta \tag{2.2}$$

where r is the distance from the probe center, m_e the electron mass, q the electron charge of an electron, ϕ the local potential, v_r the radial velocity component, and v_θ the azimuthal velocity component. Substituting equation (2.2) into equation (2.1),

we have

$$v_r^2 = \frac{2}{m_e}\left(E - q\phi - \frac{J^2}{2m_e r^2}\right). \tag{2.3}$$

In order for a particle to reach the surface of the probe, the right-hand side of equation (2.3) must be positive not only at the surface of the probe, but also all along the path from infinity to the surface. To consider the particle motion from the one dimensional viewpoint, the effective potential defined by

$$U = q\phi + \frac{J^2}{2m_e r^2} \tag{2.4}$$

should be considered. Substituting the effective potential (2.4) into (2.3), we have

$$v_r^2 = \frac{2}{m_e}(E - U). \tag{2.5}$$

By taking the effective potential as a normal potential, we can treat the 2-dimensional particle motion as the 1-dimensional case. Fig(2-1) illustrates two limits regarding the effective potential. Assume that the probe is on the left of the figure. When the sheath is thin (Langmuir Limit), the second term of equation (2.4) becomes dominant near the probe and $v(r)$ has an intermediate minimum value. For some attracted particles, this bump in the effective potential prevents them from reaching the surface even if they have enough energy. When the sheath is thick (OML limit), the first term in equation (2.4) becomes dominant throughout the region, and the electric potential is large enough to overwhelm the bump in the effective potential. Therefore the effective potential becomes monotonous, and the only requirement for a particle to reach the surface is to have a positive value of the right-hand side of equation (2.3) at the probe surface.

Electrons absorbed by the probe should be accelerated by the field force up to a certain total velocity toward the probe. Therefore, in terms of energy, it is equivalent to say,

$$\frac{1}{2}m_e(v_r^2 + v_\theta^2) + q\phi_p \geq 0 \tag{2.6}$$

where ϕ_p is the probe potential.

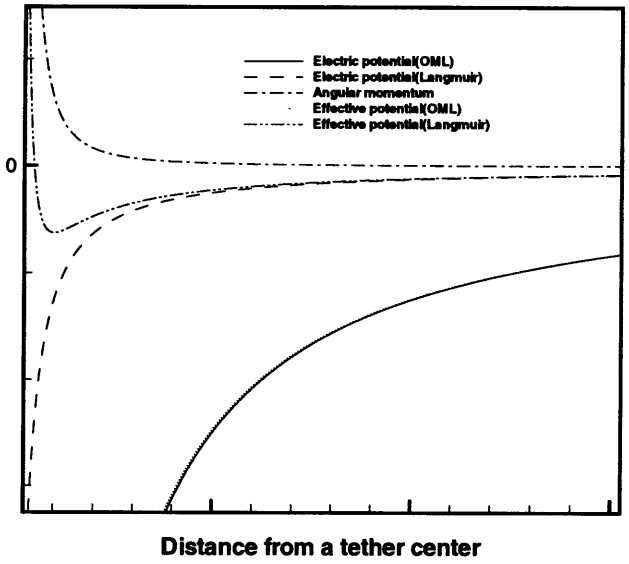

Figure 2-1: The effective potential for the thick and thin sheath

In the absence of collisions, the solution to Vlasov's equation must have the Maxwell-Boltzman form for any velocity that does occur:

$$f_e(v) = n_\infty \left(\frac{m_e}{2\pi k T_\infty}\right)^{3/2} \exp\left(-\frac{q\phi_p + \frac{m_e}{2}\left(v_\perp^2 + v_{||}^2\right)}{kT_\infty}\right) \tag{2.7}$$

where n_∞ is the density at infinity, k the Boltzmann constant, T_∞ the temperature at infinity and $v_{||}$ a velocity component parallel to the cylindrical probe.

At the surface of the probe, only electrons which satisfy the equation (2.6) can exist and be counted for the current collection. The current density into the probe is given as

$$j = q \iiint_{\frac{1}{2}m_e v_\perp^2 + q\phi_p \geq 0} f_e d\mathbf{v} \tag{2.8}$$

$$= q \int_{-\infty}^{\infty} dv_{||} \int_{\sqrt{2|q\phi_p|/m_e}}^{\infty} \int_{-\pi/2}^{\pi/2} v_\perp f_e v_\perp cos\theta d\theta dv_\perp \tag{2.9}$$

$$= \frac{q n_\infty \bar{c}_\infty}{2\sqrt{\pi}} \left[\sqrt{\frac{|q\phi_p|}{kT_\infty}} + \frac{\sqrt{\pi}}{2} e^{\frac{|q\phi_p|}{kT_\infty}} erfc\left(\sqrt{\frac{|q\phi_p|}{kT_\infty}}\right)\right] \tag{2.10}$$

$$\rightarrow \quad \frac{qn_\infty \bar{c}_\infty}{2\sqrt{\pi}} \sqrt{\frac{|q\phi_p|}{kT_\infty}} \tag{2.11}$$

since, in the limiting form, $x \rightarrow \infty$, we have

$$erfc(x) \quad = \quad 1 - erf(x) = \frac{1}{\sqrt{\pi}} \int_x^\infty e^{-t^2} dt \tag{2.12}$$

$$\rightarrow \quad \frac{2}{\sqrt{\pi}} \frac{e^{-x^2}}{x} \tag{2.13}$$

where $\bar{c}_\infty$ is the random thermal velocity given as

$$\bar{c}_\infty = \sqrt{\frac{8kT_\infty}{\pi m_e}} \tag{2.14}$$

Therefore, when $\frac{|q\phi|}{kT_\infty} >> 1$, the current density (2.13) becomes

$$j = \frac{qn_\infty}{\pi} \sqrt{\frac{2|q\phi_p|}{m_e}} \tag{2.15}$$

which is independent of electron temperature, T_e. Note that equation (2.10), and hence equation (2.15) are independent of the shape of the cylinder's cross section (as long as OML conditions prevails).

This limiting value of current density is used in this thesis as one of the criteria in the validation of our code. To see whether our code simulates plasma behavior well in the vicinity of the OML regime, we examine several Debye ratios, r_p/d_{Debye}, for the case that the ratio of the probe potential to the electron temperature, $\chi_p = \frac{|q|\phi_p}{kT_\infty}$, is 25, which case *Laframboise* has exactly computed. The solutions are available as analytical fits, which we quote in this thesis. [4, 2]

Chapter 3

Numerical Method (Particle-In-Cell)

In this chapter, the Particle-In-Cell (PIC) method used here is explained in detail. First, we introduce the structure and mechanism of the PIC method. Secondly, we describe the model for our simulation and the governing equations in a nondimensionalized form. Thirdly, we discuss the problems with the PIC method, which have occured in our application. Finally, we show the results from this simulation and compare them with the exact solutions.

3.1 Particle-In-Cell (PIC)

The Particle-In-Cell (PIC) method has been very successful in the simulation of collisionless plasmas. In PIC, many particles are distributed in phase space. That is, a particle's motion is described by its position and velocity. In kinetic theory, this particle distribution is defined as a distribution function and governed by the Boltzmann equation. The Boltzmann equation with no collisional term on its right-hand side is given as follows. (Vlasov's equation)

$$\frac{\partial f}{\partial t} + \mathbf{v}\frac{\partial f}{\partial \mathbf{x}} + \mathbf{F}\frac{\partial f}{\partial \mathbf{v}} = 0 \tag{3.1}$$

In an actual computation, the number of particles available is much less than that in reality. This fact requires us to introduce the concept of a "superparticle", corresponding to a group of real particles. One superparticle contains many real particles, and as many particles as another.

To describe the motion of the superparticle, we need to know velocity and the force acting on it. The force acting on a superparticle can be calculated by considering all Lorentz forces caused by the other superparticles. However, this calculation is computationally too expensive. Instead of doing so, PIC uses a grid on which Maxwell's equations are solved to give the electric field, which is then interpolated to the position of each superparticle. As the name "Particle-In-Cell" implies, in a computational domain, a superparticle moves through a grid or a cell, regardless the position of grid nodes. A PIC code method consists of four processes as described below.

At each time step, the electric charge density on each node is estimated from the positions of all superparticles. This first process is called "charge assignment". Then on a grid, the electric potential and electric field are computed. We use a finite difference method in this second process; especially to solve Poisson's equation, we use Successive Line OverRelaxation (SLOR). Poisson's equation to relate electric potential to charge density is

$$\nabla^2\phi = -\frac{\rho}{\epsilon} \tag{3.2}$$

where $\rho = |q|(n_i - n_e)$ is the electric charge density , and the electric field is

$$\mathbf{E} = -\nabla\phi. \tag{3.3}$$

if $\frac{\partial \mathbf{B}}{\partial t}$ can be neglected.

After computing $\mathbf{E}$ on a grid, the electric field is interpolated onto each superparticle's position, and the corresponding force and acceleration of a superparticle is calculated. This third process is called "interpolation". The first and third process involve the same weighting method to avoid the so-called "self force". Once we know the acceleration, a leapfrog method, the final process, updates the velocity and

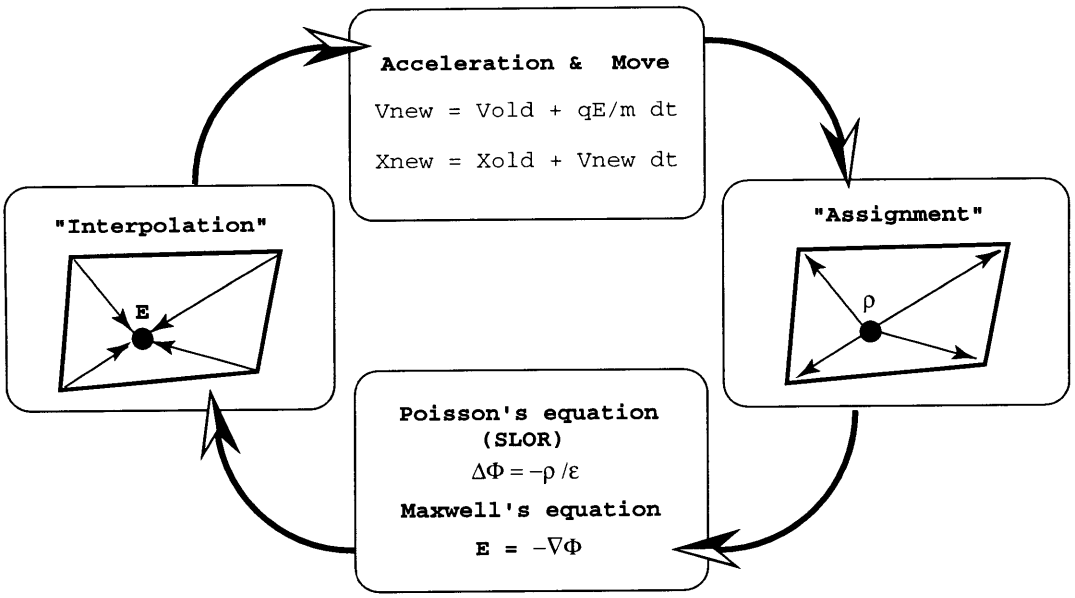

Figure 3-1: A typical cycle of PIC

position of each superparticle as follows;

$$\mathbf{v}_{new}^{(n)} = \mathbf{v}_{old}^{(n-1)} + \frac{q\mathbf{E}^{(n-1/2)}}{m}\Delta t \tag{3.4}$$

$$\mathbf{x}_{new}^{(n+1/2)} = \mathbf{x}_{old}^{(n-1/2)} + \mathbf{v}_{new}^{(n)}\Delta t. \tag{3.5}$$

This completes one iteration in a PIC calculation. One cycle of a PIC is shown skematically in fig 3-1.

3.2 Simulation Model

This section explains the simulation model. We wish to calculate the electron current collection by a positively charged cylindrical tether in a quiescent unmagnetized plasma in a Maxwellian collisionless condition. For simplicity, we first nondimensionalize the governing equations.

Non-dimensionalization

Before we consider the non-dimensionalization, we should know what equations are involved in our simulation. As we showed before, the leapfrog method uses equations

(3.4) and (3.5). To solve for electric field from electric charge density, we use Poisson's equation (3.2) and Maxwell's equation (3.3). Essentially, these four equations are the governing equations. Since we are not directly solving Boltzmann's equation (3.1), it is not considered as a governing equation. The distribution function, however, should be considered. A Maxwellian distribution function is used to calculate the number of particles replenished into the computational domain at each timestep and the density at the outside boundary.

In non-dimensionalizing the governing equations, we use reference values as follows;

Length	: $l_{ref} = d_{Debye} = \sqrt{\frac{\epsilon k T_e}{q^2 n_\infty}}$
Time	: $t_{ref} = 10/\omega_p$ $(\omega_p = \sqrt{\frac{q^2 n_\infty}{\epsilon m_e}})$
Potential	: $\phi_{ref} = \frac{kT_\infty}{e}$
Density	: $n_{ref} = n_\infty/100$
Velocity	: $v_{ref} = l_{ref}/t_{ref} = v_T/10 = \sqrt{\frac{kT_e}{m_e}}/10$
Distribution function	: $f_{ref} = n_{ref}/v_{ref}^3$.

As is discussed later, somehow strange reference values seen here is totally due to the computational limitations.

Substituting these reference values, we nondimensionalize equations (3.2), (3.3),(3.4),(3.5) and (2.7).

$$\hat{\nabla}^2\hat{\phi} = -(\hat{n_i} - \hat{n_e})/100 \tag{3.6}$$

$$\hat{\mathbf{E}} = -\hat{\nabla}\hat{\phi} \tag{3.7}$$

$$\hat{\mathbf{v}}_{new} = \hat{\mathbf{v}}_{old} \pm 100(\frac{m_e}{m})\hat{\mathbf{E}}d\hat{t} \tag{3.8}$$

$$\hat{\mathbf{x}}_{new} = \hat{\mathbf{x}}_{old} + \hat{\mathbf{v}}_{new}d\hat{t} \tag{3.9}$$

$$\hat{f} = \frac{1}{10(2\pi)^{3/2}} \exp\left(-50\hat{v}^2 - \hat{\phi}\right) \tag{3.10}$$

where a hat ($\hat{}$) indicates a nondimensional quantity. In equation (3.8), the minus sign is taken when the particle is an electron ($m = m_e$), and the plus when an ion ($m = m_i$).

In this simulation, we use the parameters in Table 3.1. In deciding these values,

Electron Temperature	$\hat{T}_e = 100$
Ion Temperature	$\hat{T}_i = 100$
Electron density	$\hat{n}_e = 100$
Ion density	$\hat{n}_i = 100$

Table 3.1: Parameters

we first consider the number of particles available in a computer memory. In order to include the sheath region completely, we have the radius of the computational domain as $15d_{Debye}$. To be consistent with the governing equations and these non-physical values, we calculate other nondimensionalized variables, starting with the Debye length equal to unity,

$$\begin{aligned} \hat{d}_{Debye} &= \sqrt{\frac{\epsilon kT}{q^2 n}}/l_{ref} \\ &= 1.0 \end{aligned} \tag{3.11}$$

Since the area of the computational domain is $(15\hat{d}_{Debye})^2\pi$, we need approximately $\hat{n}_{e,i}(15\hat{d}_{Debye})^2\pi$ particles for each species. This number is limited by the computer. In our case, the number of particles available is about $200,000$. In order to run the simulation with as many particles as possible but less than this, we set $\hat{n}_{e,i} = 100$. From equation (3.11), we also have the temperature, $\hat{T}_{i,e} = 100$. Consequently, we have the thermal velocity,

$$\begin{aligned} \hat{v}_T &= \sqrt{\frac{kT}{m}}/v_{ref} \\ &= \sqrt{100} \end{aligned} \tag{3.12}$$

and the plasma frequency,

$$\begin{aligned} \hat{\omega}_p &= \sqrt{\frac{q^2 n}{\epsilon m}} t_{ref} \\ &= \sqrt{100}. \end{aligned} \tag{3.13}$$

As we can see now, the factors seen in the reference values are determined by the computational limitations.

We should note that we use hypothetically light ion's mass, which is the same as an electron's mass. We discuss the validity of this hypothesis and its effect on the computational cost later. Physically, since almost no ions are lost to the probe, all velocities are possible everywhere, and their distribution is, in fact, a full Maxwell-Boltzmann distribution, so that the ion density is simply $n_i = n_\infty \exp(-\frac{|q|\phi}{kT_i})$, which does not depend on m_i at all.

Mesh

In our code, the Debye length is first determined. Therefore, for various cases of Debye ratio, i.e. the ratio of the tether radius to the Debye length, different meshes are used. The mesh used for the case of the Debye ratio equal to 1, $\xi_p = 1$, is shown in Figure 3-2. Each mesh size in the radial direction is kept to be a half of the Debye length and in the azimuthal direction mesh size is kept less than the Debye length, which should avoid numerical instabilities.

The main purpose of this simulation is to calculate how many particles, mainly electrons, are collected by a cylindrical tether in a Maxwellian collisionless condition. Particles are counted and absorbed when they reach the surface of the tether. From outside of the computational domain, where plasma is assumed to be Maxwellian, electrons and ions are replenished into the domain with velocity and position calculated from the Maxwellian distribution function using a random number generator.

3.3 Problems in PIC

As we have applied the PIC method, we have been confronted with some problems. In this section, we discuss those problems and some solutions to them.

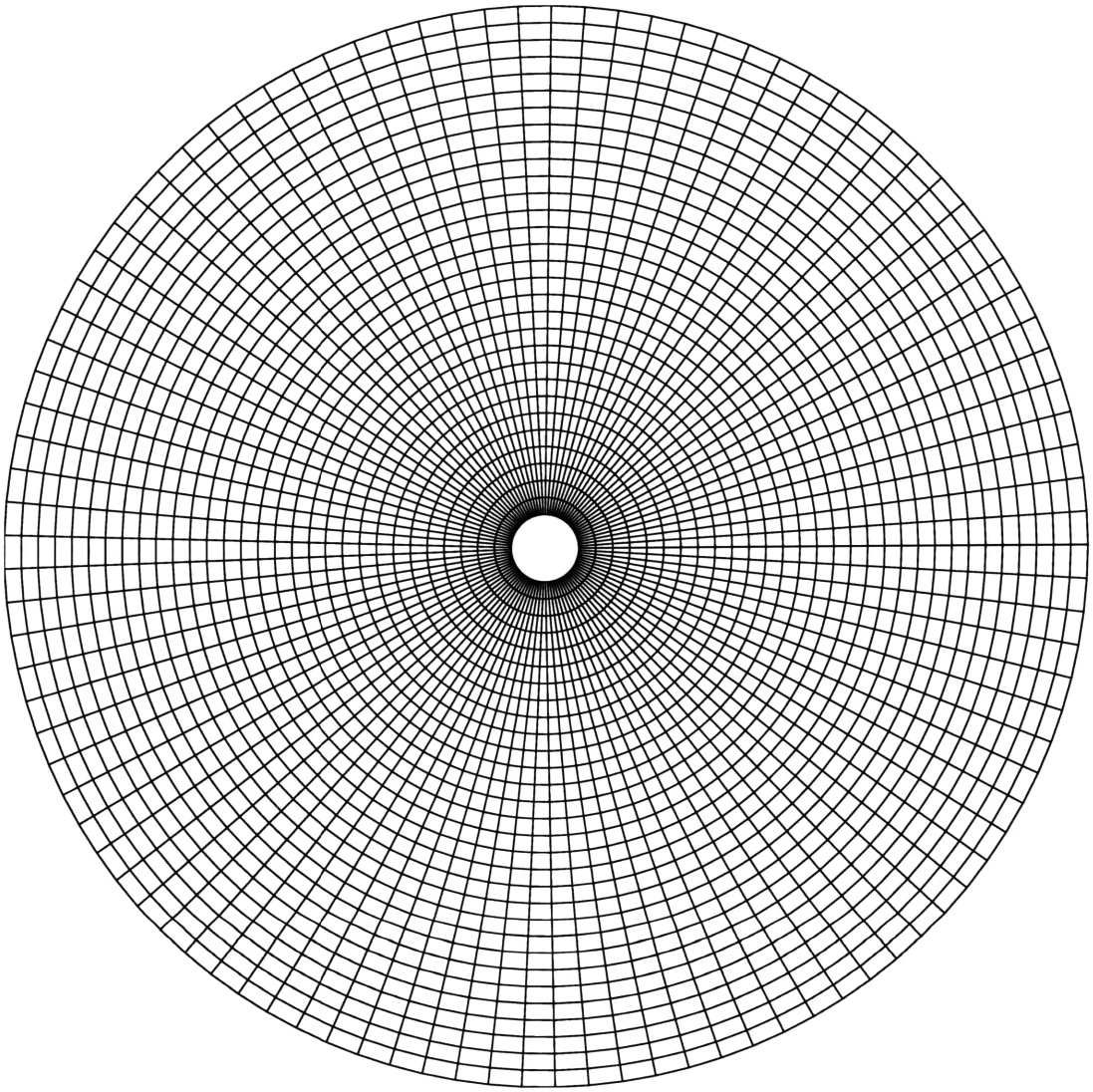

Figure 3-2: Mesh for the case $\xi_p = \frac{r_p}{d_{Debye}} = 1$

3.3.1 Deformed Grid

As we consider some practical configurations in engineering applications, it is almost impossible to do it with only a rectangular grid. The more complicated the configuration becomes, the more necessary it is to use a deformed body-fitted grid. Concerning this problem, we can think of two factors of a deformed grid, which are likely to cause problems, namely the area of the cell and the degree of deformity from a rectangle.

First, we describe the mechanism of the "assignment" and "interpolation" processes. In the original PIC method based on a rectangular grid, electric charge density is first calculated from the particle position and assigned to four nodes according to the area-weighting function. The area-weighting function is defined as follows.

Uniform rectangular grid

A particle with electric charge q is located at (x, y) in a cell of area A, which is defined by four nodes (x_i, y_i), $(x_i + \Delta x, y_i)$, $(x_i, y_i + \Delta y)$ and $(x_i + \Delta x, y_i + \Delta y)$. That is, the area A is given as

$$A = \Delta x \Delta y. \tag{3.14}$$

First, we calculate the electric charge density, by dividing q by the area, $\Delta x \Delta y$.

$$\rho = \frac{q}{\Delta x \Delta y} \tag{3.15}$$

Next, we split this charge density into four segments, which are proportional to the area demarcated by lines parallel to grid edges. Thus, to point $A(x_i, y_i)$, charge density

$$\rho_A = \rho \frac{\square PFCG}{\square ABCD} = q \frac{(x_{i+1} - x)(y_{i+1} - y)}{\Delta x^2 \Delta y^2} \tag{3.16}$$

is assigned. Likewise, to the other points, we assign charge density as

$$\rho_B = \rho \frac{\square PGDH}{\square ABCD} = q \frac{(x - x_i)(y_{i+1} - y)}{\Delta x^2 \Delta y^2} \tag{3.17}$$

$$\rho_C = \rho \frac{\square PHAE}{\square ABCD} = q \frac{(x - x_i)(y - y_i)}{\Delta x^2 \Delta y^2} \tag{3.18}$$

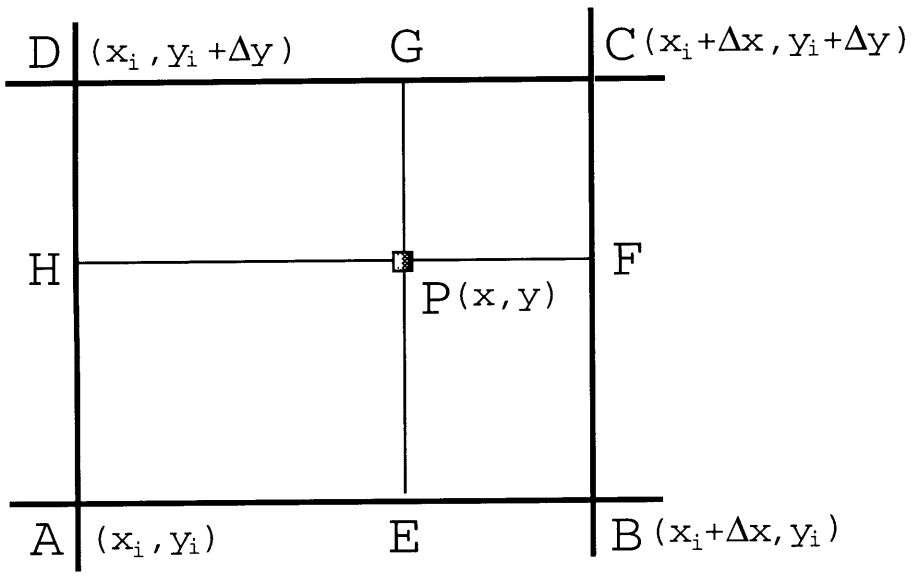

Figure 3-3: A uniform rectangular grid

$$\rho_D = \rho\frac{\square PEBF}{\square ABCD} = q\frac{(x_{i+1}-x)(y-y_i)}{\Delta x^2 \Delta y^2} \tag{3.19}$$

This assignment process is applied to all particles in the cell $ABCD$.

We next estimate the order of accuracy of this assignment method. To exclude the effects of an insufficient number of particles, we assume that there is a sufficient number of particles in a cell. This condition is expressed by requiring the density to be a continuous function. When we consider a small element in the cell, the condition requires that there be still many particles in it.

Let $f(x,y)$ be the superparticle density function at (x,y), and $dxdy$ be the area of the small element. The condition to have a sufficient number of particles requires

$$f(x,y)dxdy \geq 1 \tag{3.20}$$

Assuming a large enough number of particles in a cell and using the Taylor series expansion, we estimate the order of accuracy at the node A. One assignment process is applied at once to all particles in the small element. Since the element is taken to be very small, we can consider that there are $f(x,y)dxdy$ particles at (x,y). The

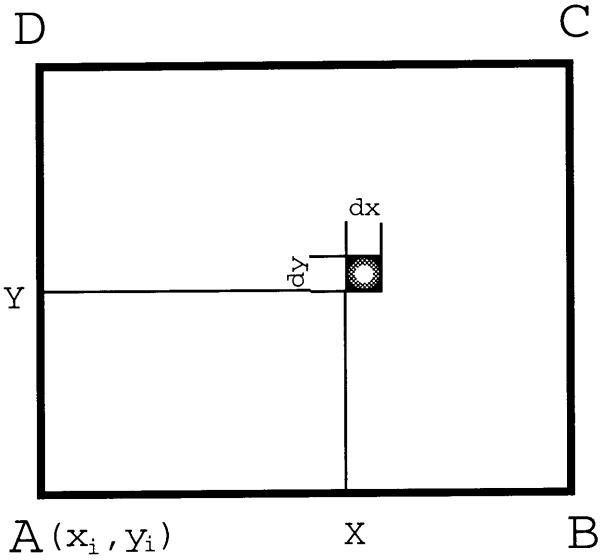

Figure 3-4: A small element in a cell

assigned charge density at A from those particles' point (x, y) is given by

$$d\rho_A(x,y) = \frac{q(x_{i+1}-x)(y_{i+1}-y)}{\Delta x^2 \Delta y^2} f(x,y)dxdy. \tag{3.21}$$

Assigning all particles in a whole cell to the node A, we have,

$$\begin{aligned}
\rho_A &= \int_{x_i}^{x_{i+1}} \int_{y_i}^{y_{i+1}} d\rho_A(x,y) && (3.22)\\
&= \int_{x_i}^{x_{i+1}} \int_{y_i}^{y_{i+1}} \frac{q(x_{i+1}-x)(y_{i+1}-y)}{\Delta x^2 \Delta y^2} f(x,y)dxdy && (3.23)\\
&= \int_0^1 \int_0^1 q(1-X)(1-Y)g(X,Y)dXdY && (3.24)
\end{aligned}$$

where $X = \frac{x-x_i}{\Delta x}$, $Y = \frac{y-y_i}{\Delta y}$ and $g(X,Y) = f(x_i + \Delta x X, y_i + \Delta y Y)$. Expanding $g(X,Y)$ around the point $(0,0)$,

$$\begin{aligned}
g(X,Y) &= g(0,0) + \left.\frac{\partial g}{\partial X}\right|_{(0,0)} X + \left.\frac{\partial g}{\partial Y}\right|_{(0,0)} Y + \cdots && (3.25)\\
&= f(x_i,y_i) + \left.\frac{\partial f}{\partial x}\right|_{(x_i,y_i)} \Delta x\, X + \left.\frac{\partial f}{\partial y}\right|_{(x_i,y_i)} \Delta y\, Y \cdots && (3.26)
\end{aligned}$$

and substituting this into equation (3.24), we have

$$\begin{aligned}\rho_A &= q\int_0^1\int_0^1 [f(x_i,y_i)(1-X)(1-Y) \\ &\quad + \left.\frac{\partial g}{\partial X}\right|_{(0,0)} X(1-X)(1-Y) + \left.\frac{\partial g}{\partial Y}\right|_{(0,0)} Y(1-X)(1-Y) + \cdots]dXdY \quad (3.27) \\ &= \frac{q}{4}f(x_i,y_i) + \frac{q}{12}\left.\frac{\partial f}{\partial x}\right|_{(x_i,y_i)}\Delta x + \frac{q}{12}\left.\frac{\partial f}{\partial y}\right|_{(x_i,y_i)}\Delta y + \cdots \quad (3.28)\end{aligned}$$

Performing the same calculation for all particles in the other cells which surround the node A, we can cancel the 2nd and 3rd terms and get

$$\rho_A = qf(x_i,y_i) + O(\Delta x^2, \Delta y^2). \quad (3.29)$$

This shows that, as long as there are a sufficient number of particles, this area-weighting assignment method provides 2nd order of accuracy.

Rectangular grid with different cell sizes

Next, following the same procedure, we consider the effect of rectangular cells of different sizes on the assignment method (fig 3-5). When the cells are of different sizes but still rectangular, the 2nd and 3rd terms in equation (3.28) do not cancel out after the summation of corresponding terms from other cells. Instead of the second order of accuracy, we get

$$\begin{aligned}\rho_A &= qf(x_i,y_i) \\ &\quad + \frac{q}{6}\left.\frac{\partial f}{\partial x}\right|_{(x_i,y_i)}(\Delta x_1 - \Delta x_2) + \frac{q}{6}\left.\frac{\partial f}{\partial y}\right|_{(x_i,y_i)}(\Delta y_1 - \Delta y_2) \\ &\quad + O(\Delta x^2, \Delta y^2), \quad (3.30)\end{aligned}$$

which provides 1st order of accuracy only.

As we can see from the 2nd and 3rd terms in equation (3.30), using almost the same shape and size as those of adjacent cells, we can make these terms quite small, and make this method closer to second order of accuracy.

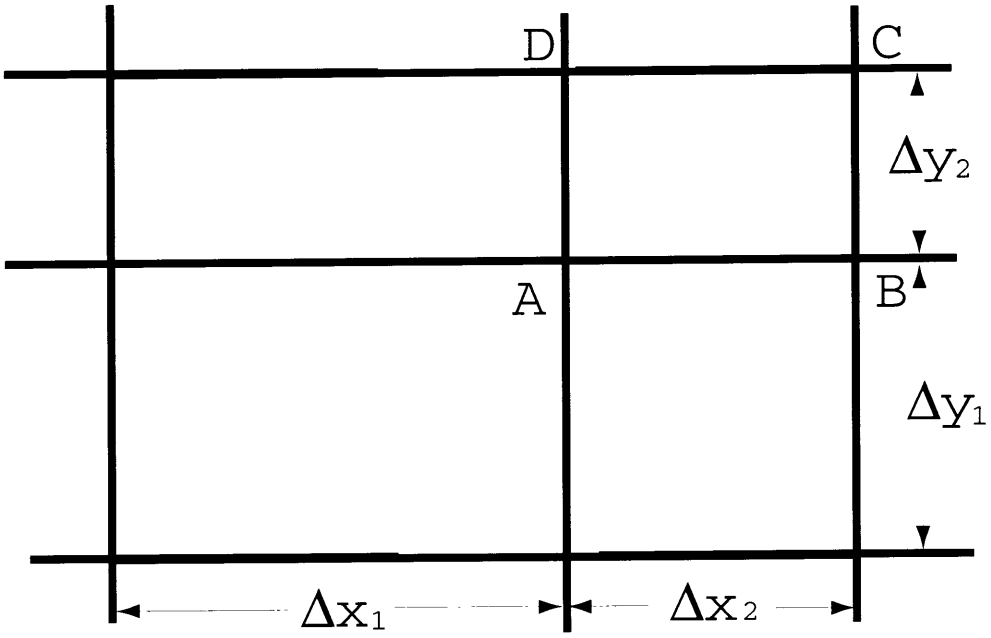

Figure 3-5: Cells of different sizes

Deformed grid

Next we consider the deformity of a grid. Since we use a linear interpolation [8, 7] from a deformed grid to a square grid on which the area-weighting is performed, we can not avoid a problem due to this deforming. In our code, we use the typical tri-linear interpolation from the physical domain (x, y) to the computational domain (r, s) given as

$$x = x_0 + x_1 r + x_2 s + x_3 rs \tag{3.31}$$

$$y = y_0 + y_1 r + y_2 s + y_3 rs \tag{3.32}$$

where

$$x_0 = x_{i,j}$$

$$y_0 = y_{i,j}$$

$$x_1 = x_{i+1,j} - x_{i,j}$$

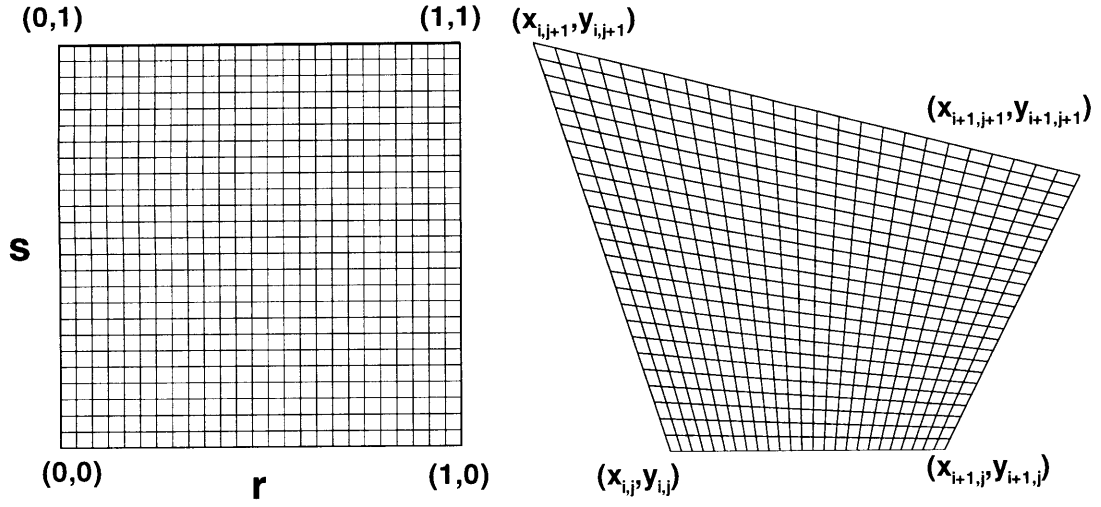

Figure 3-6: Transformed square grid (left) and the original deformed grid (right)

$$
\begin{aligned}
y_1 &= y_{i+1,j} - y_{i,j} \\
x_2 &= x_{i,j+1} - x_{i,j} \\
y_2 &= y_{i,j+1} - y_{i,j} \\
x_3 &= x_{i+1,j+1} + x_{i,j} - x_{i+1,j} - x_{i,j+1} \\
y_3 &= y_{i+1,j+1} + y_{i,j} - y_{i+1,j} - y_{i,j+1}
\end{aligned}
$$

The effect of the linear interpolation is understood when we look at Figure 3-6.

In a deformed cell, the grid density is sparser at the top and denser at the bottom. But its corresponding square cell has a completely uniform density distribution. This means that if we start for example with a particle distribution which is uniform in the grid on the left, it will not be uniform in the one on the right, and vice versa. Although we have no particular treatment done to solve this problem in our simulation, as seen in the grid we use (fig. 3-2) , each cell is almost rectangular. Therefore, no serious error can be considered to be incurred due to the deformity of the cell. Moreover, in the grid no pair of adjacent cells has a significant difference in size and shape. This makes the assignment method to be close to 2nd order accurate.

3.3.2 Boundary Condition

In this section, we consider the outside boundary condition in our simulation. The importance of this boundary condition stems from the fact that some electrons are absorbed by a tether. We assume here that no ion is absorbed by the tether, because of its very high positive potential. Figure 3-7 illustrates the overall flow of electrons and ions. Due to this partial absorption of electrons by the tether, the electric potential at the computational outside boundary can not be zero with respect to the ambient plasma. If it were zero, the electron density would be less than the ion density, and thus it would violate the quasi-neutrality outside the sheath. To maintain the quasi-neutrality, the electron potential at the outside boundary should be more than zero. Positive potential attracts more electrons and fewer ions. This boundary condition is formulated as follows.

Let ϕ be the electric potential at an arbitrary point including the outside boundary. Assuming that ions are singly charged, we have the quasi-neutrality equation as

$$|n_e - n_i| \ll n_e. \tag{3.33}$$

In the computation, we use this condition in the form of

$$n_e = n_i. \tag{3.34}$$

However this does not allow us to transform Poisson's equation to Laplace's equation by equating the source term to zero, because the small difference $|q|(n_i - n_e)$ is divided by the small quantity ϵ_0, leaving $\nabla^2\phi$ indeterminate. As the plasma approximation claims, plasma tends to neutralize itself by imposing $n_e = n_i$. Therefore we impose the condition (3.34) on the outside boundary, and solve Poisson's equation inside that boundary only with non-zero source term on its right-hand side.

To determine the boundary condition, we need the potential, which is calculated as follows. The assumption that no ions are absorbed by the tether enables us to calculate the ion density at any point. Given the ion temperature, T_i and the potential,

ϕ, and integrating the Maxwell-Boltzmann distribution function in velocity space, we have the ion density as

$$n_i = n_\infty \exp(-\frac{|q|\phi}{kT_i}) \tag{3.35}$$

On the other hand, we can calculate only the density of inbound electrons[1]. Since some electrons are absorbed, we do not know the limits of outbound electron distribution function in phase space. We denote the density of those outbound electrons as n_e^{out}. As for the inbound electron density, we can calculate it by integrating the Maxwellian distribution, since all those electrons can be tracked back to infinity, where the Maxwellian distribution prevails. The inbound electron density is given at any radius by

$$\begin{aligned} n_e^{in} &= \int_{-\infty}^{\infty}\int_{\pi/2}^{\pi/2}\int_{\sqrt{|q|\phi/m_e}}^{\infty} n_\infty \left(\frac{m_e}{2\pi kT}\right)^{3/2} \exp\left(-\frac{\frac{1}{2}m_e(v^2+v_z^2)+q\phi}{kT}\right) v\cos\theta dv d\theta dv_z \\ &= \frac{n_\infty}{2}. \end{aligned} \tag{3.36}$$

Substituting (3.35) and (3.36) into (3.34), Then, we have

$$n_e^{out} + \frac{n_\infty}{2} = n_\infty \exp(-\frac{|q|\phi}{kT}) \tag{3.37}$$

Given the outbound electron density at the outside boundary, equation (3.37) allows us to calculate the potential there.

The outbound electron density, n_e^{out} is calculated computationally by considering the outbound flux, $\mathbf{\Gamma}$. The flux through the boundary is given by

$$\mathbf{\Gamma} = n_e^{out} v_e^{out} \tag{3.38}$$

where v_e^{out} is the flow velocity due to the outbound electrons, that is, the average

[1]In this thesis, we call a particle which is coming into the computational domain, an "inbound" particle, and one going out of the domain, an "outbound" particle.

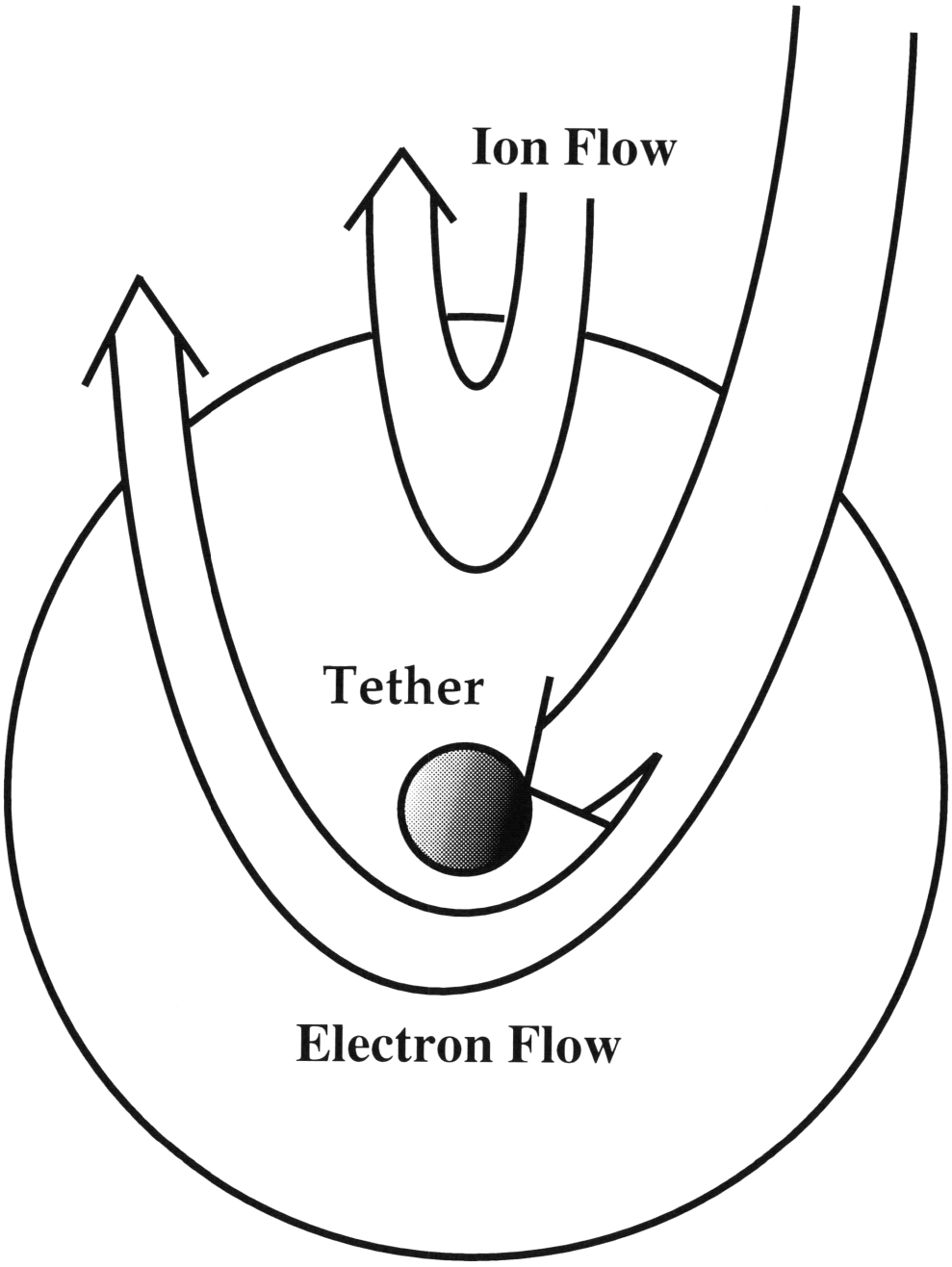

Figure 3-7: Electron and Ion Flow

velocity normal to the boundary, given as

$$v_e^{out} = \frac{\sum_{i=1}^{k} \mathbf{w}_{ei} \cdot \mathbf{n}_i}{k} \tag{3.39}$$

where k is the number of electrons counted as they cross the boundary, $\mathbf{n}_i$ the normal vector to the boundary and $\mathbf{w}_{ei}$ the particle velocity. The number of electrons which go out of the domain, k, is

$$k = \mathbf{\Gamma} dt S \tag{3.40}$$

where dt is the timestep and S is the area of the outside boundary. Substituting (3.40) and (3.39) into (3.38), we have the outbound electron density as

$$n_e^{out} = \frac{k^2}{\sum_{i=1}^{k} \mathbf{w}_{ei} \mathbf{n}_i dt S} \tag{3.41}$$

Now we are ready to calculate how many electrons and ions are to be replenished at each timestep. The number of those particles is calculated by multiplying the flux by the timestep and the area of the outside boundary. The number of electrons to be replenished, k_e, is given

$$\begin{aligned} k_e &= \int_{-\infty}^{\infty}\int_{\pi/2}^{\pi/2}\int_{\sqrt{|q|\phi/m_e}}^{\infty} n_\infty \left(\frac{m_e}{2\pi kT}\right)^{3/2} \exp\left(-\frac{\frac{1}{2}m_e(v^2+v_z^2)+q\phi}{kT}\right) v^2 \cos\theta dv d\theta dv_z S dt \\ &= \frac{n_\infty \bar{c}_\infty}{4}\left\{\frac{2}{\sqrt{\pi}}\sqrt{\frac{|q|\phi}{kT}} + \exp\left(\frac{|q|\phi}{kT}\right) erfc\sqrt{\frac{|q|\phi}{kT}}\right\} S dt \end{aligned} \tag{3.42}$$

where $\bar{c}_\infty$ is the random thermal velocity given in equation (2.14). It should be noted that this is the same as equation (2.10), except for ϕ instead of ϕ_p. And the number of ions to be replenished, k_i, is given

$$\begin{aligned} k_i &= \int_{-\infty}^{\infty}\int_{\pi/2}^{\pi/2}\int_{0}^{\infty} n_\infty \left(\frac{m_i}{2\pi kT}\right)^{3/2} \exp\left(-\frac{\frac{1}{2}m_i(v^2+v_z^2)+q\phi}{kT}\right) v^2 \cos\theta dv d\theta dv_z S dt \\ &= 2n_\infty \left(\frac{kT}{2\pi m_i}\right)^{1/2} \exp\left(-\frac{|q|\phi}{kT}\right) S dt \end{aligned} \tag{3.43}$$

In the simulation, a random number generator is used to locate the place to be

replenished and provide the particle with a velocity estimated from the Maxwellian distribution function.

3.3.3 Computational Cost

In order to resolve the non-neutral domain, namely a sheath domain, both electrons and ions should be moved. Typically, heavy, slow ions require very long computational time till the ion distribution has converged. To speed up this computation, we use hypothetically light ions, which have the same mass as electrons. The use of such a light ion is justified by the fact that we are only interested in the ion density, and the assumption that no ion is absorbed by the tether and hence that the ion's distribution function is Maxwellian. From this assumption, we can show that the ion density does not depend on the ion mass. That is,

$$\begin{aligned} n_i &= \int_{-\infty}^{\infty} n_\infty \left(\frac{m_i}{2\pi kT}\right)^{3/2} \exp\left(-\frac{\frac{1}{2}m_i\mathbf{v}^2 + |q|\phi}{kT}\right) d\mathbf{v} \\ &= n_\infty \exp\left(-\frac{|q|\phi}{kT}\right), \end{aligned} \tag{3.44}$$

This fact enables us to use the very light ion, with which the computation gives the ion density in the computational domain. We should note here that the trajectory of light ions is different from that of real ions, but the corresponding density is the same. Actually with these light ions ($m_i = m_e$), we can get the same result as with other ion mass, say $m_i = 1840m_e$, and that more than 5 times as fast.

3.4 Results

In this section, we show the results from our simulation. First, to check our simulation qualitatively, we show and examine the field quantities. In Figures 3-8, 3-9, and 3-10, instantaneous charge densities for the cases of the Debye ratio equal to 1, 2 and 5 are shown. As we would expect, in the vicinity of the tether, there is a region where electrons are dominant and quasi-neutrality no longer prevails. This region is the

"sheath".

From this electric charge density, we solve by Successive Line OverRelaxaion (SLOR) to obtain the electric potential distributions, which are shown in Figure 3-11, 3-12 and 3-13 for the same cases. These figures clearly illustrate the sheath region in the vicinity of the tether. The electric potential there is positive, indicating the non-neutrality.

Next we examine the quantitative result from the simulation. Figure 3-14 shows the history of current collected by the tether and the corresponding value from the results of *Laframboise*. After some perturbation, the observed current oscillates just below the *Laframboise*'s value. This oscillation is attributed to the small timestep and the small number of particles used in this simulation. The reason why the current collection in the case of $\xi_p = 1$ has a larger amplitude than the others is that the surface area of the tether is smaller than that of the others and thus one particle difference becomes more significant to the current density calculation.

The consistent negative bias in the result (about 7%) is probably due to the grid distortion, as noted before. But more work needs to be done to verify this.

Finally, the figure 3-15 shows the comparison of the current collection obtained in the simulation with the analytical values for different cases of the Debye ratio. From this figure, the PIC method is verified to give the same trend of the analytical solution. In the figure 3-15, current collected is normalized by the random thermal current given by

$$I = Sn_\infty |q| \sqrt{\frac{kT_{i,e}}{2\pi m_{i,e}}} \tag{3.45}$$

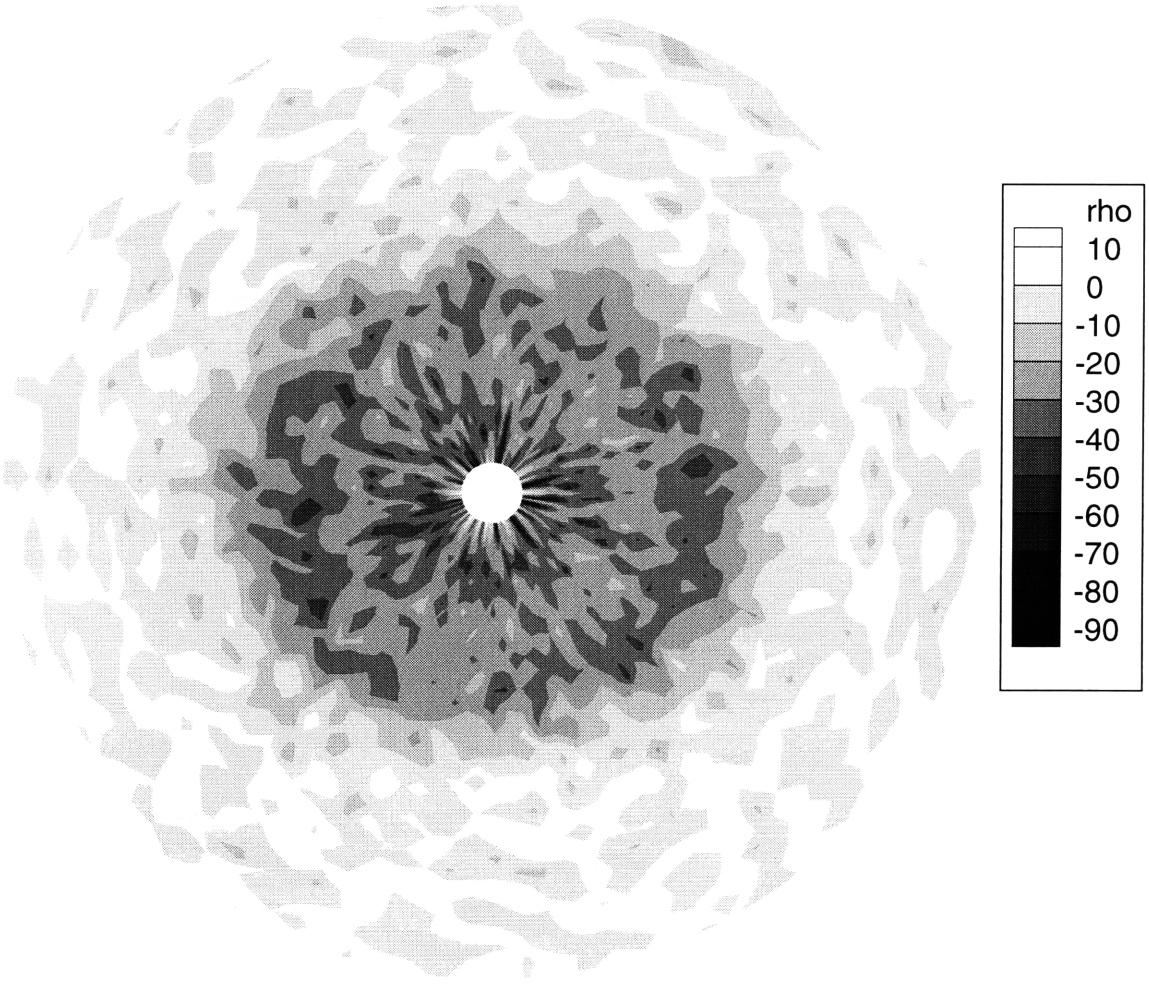

Figure 3-8: Electric charge density for the case $\xi_p = 1$

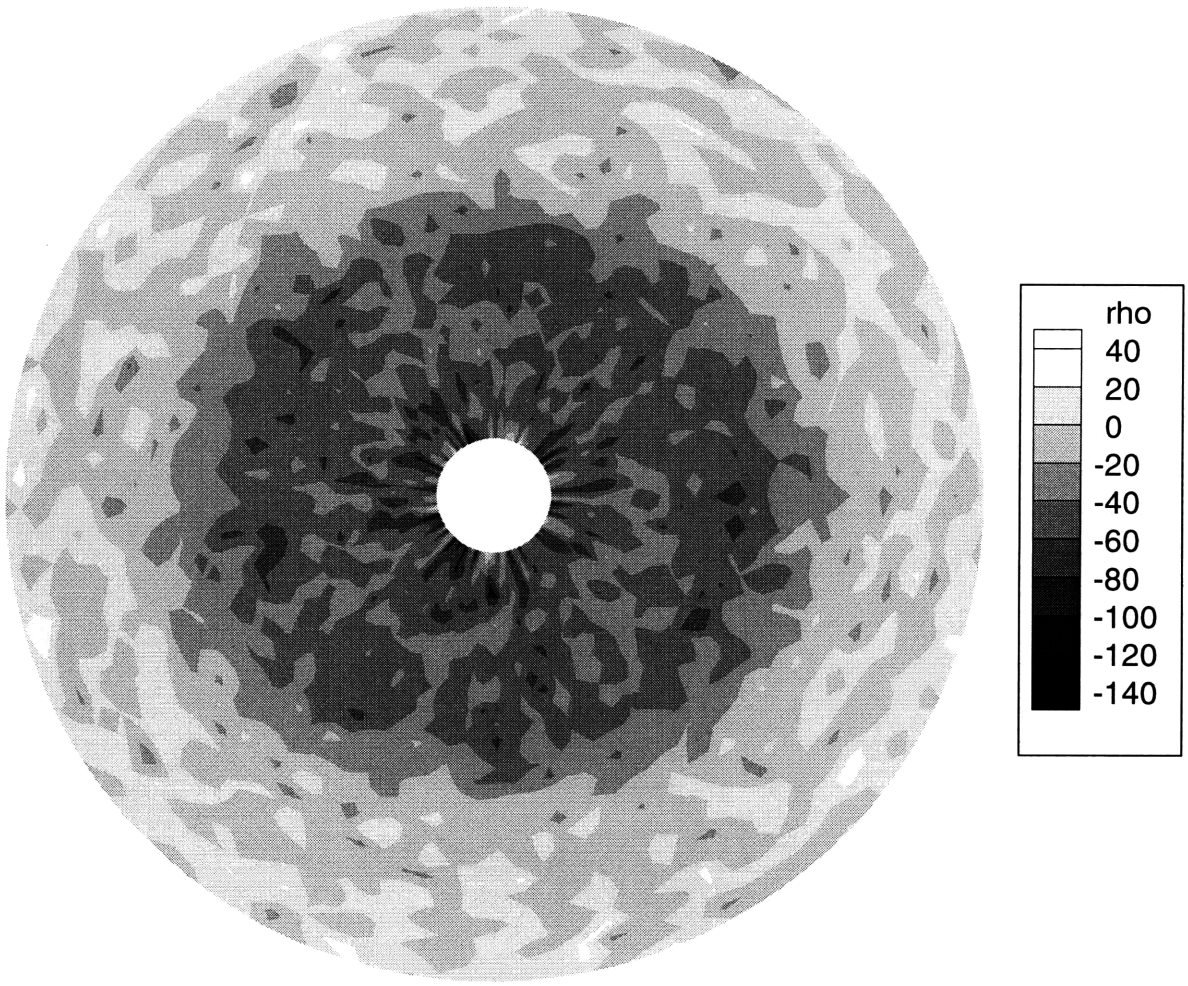

Figure 3-9: Electric charge density for the case $\xi_p = 2$

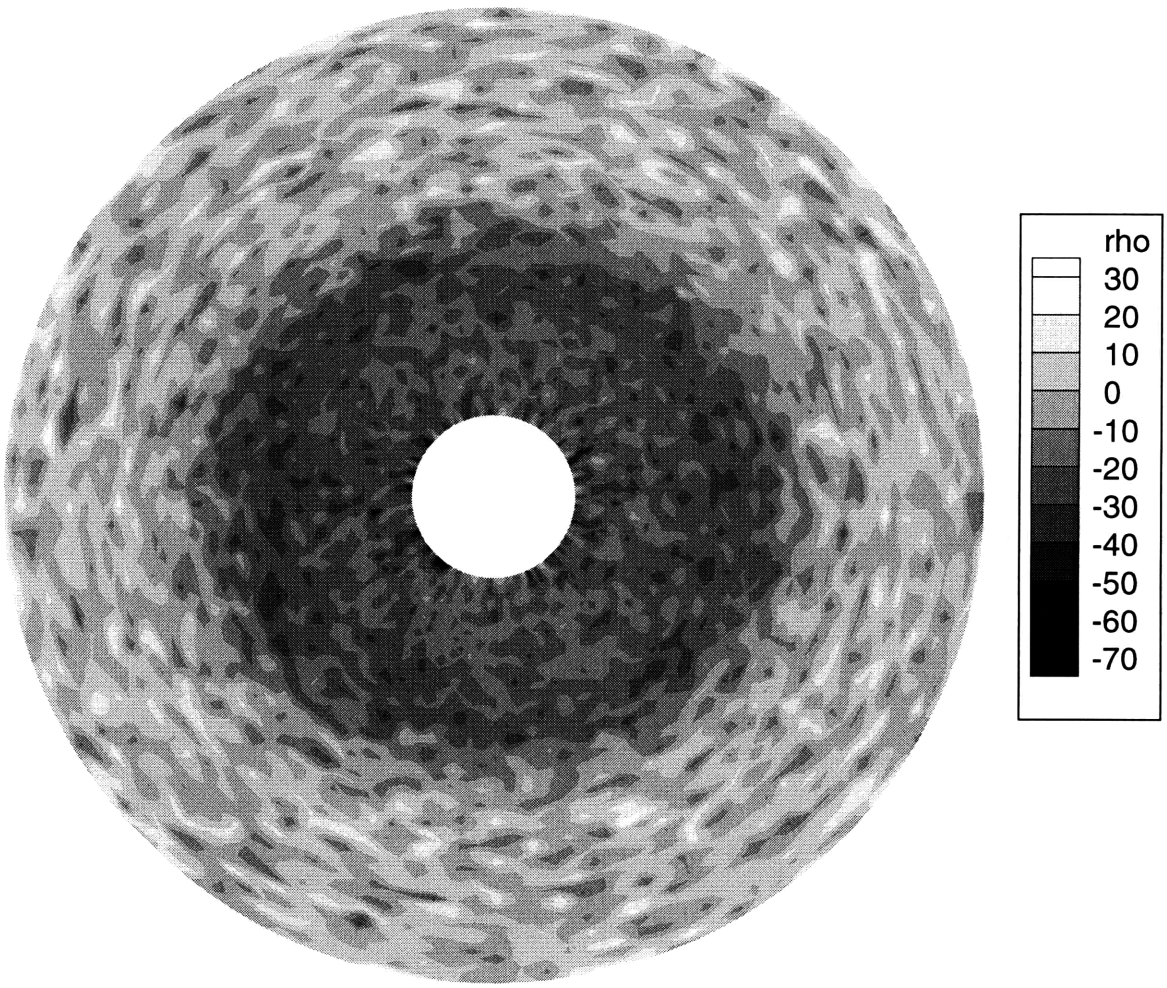

Figure 3-10: Electric charge density for the case $\xi_p = 5$

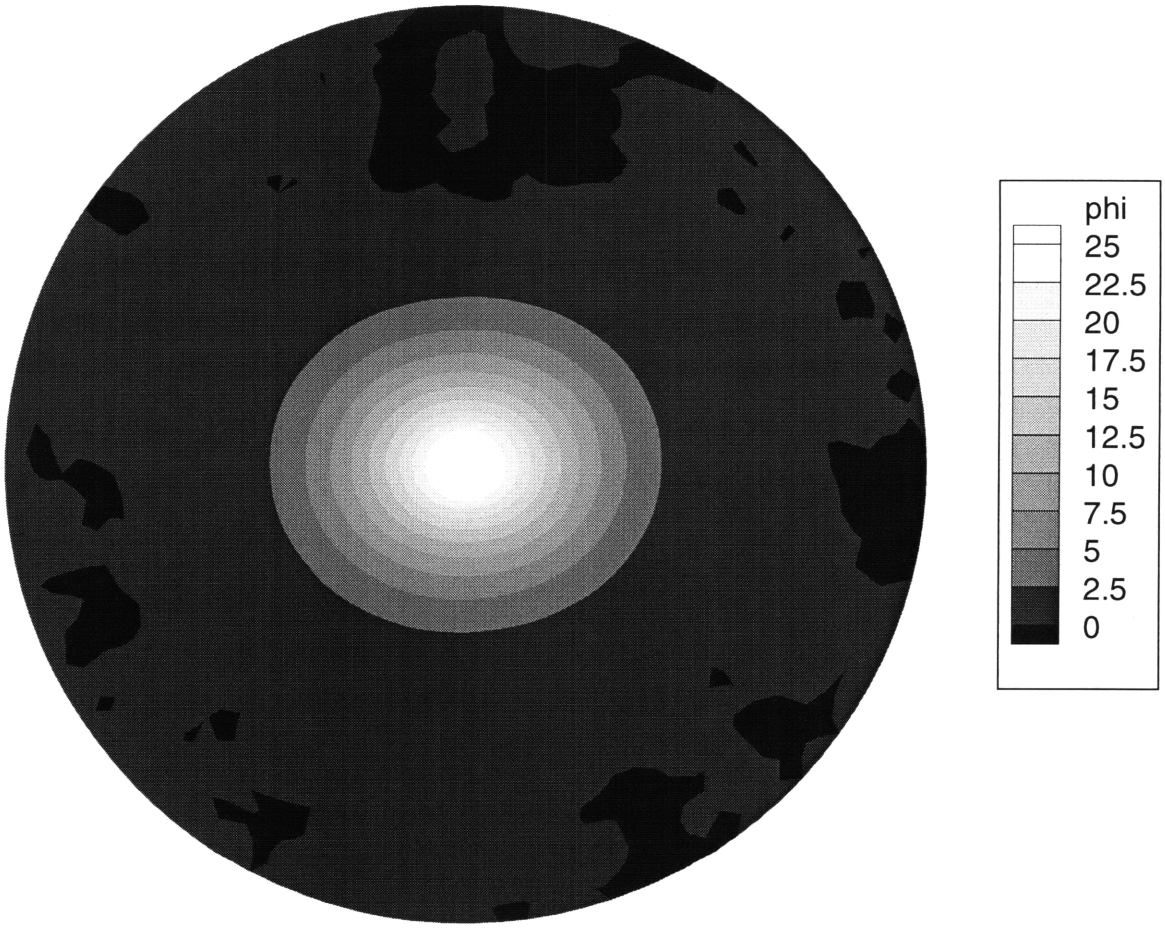

Figure 3-11: Electric potential distribution for the case $\xi_p = 1$

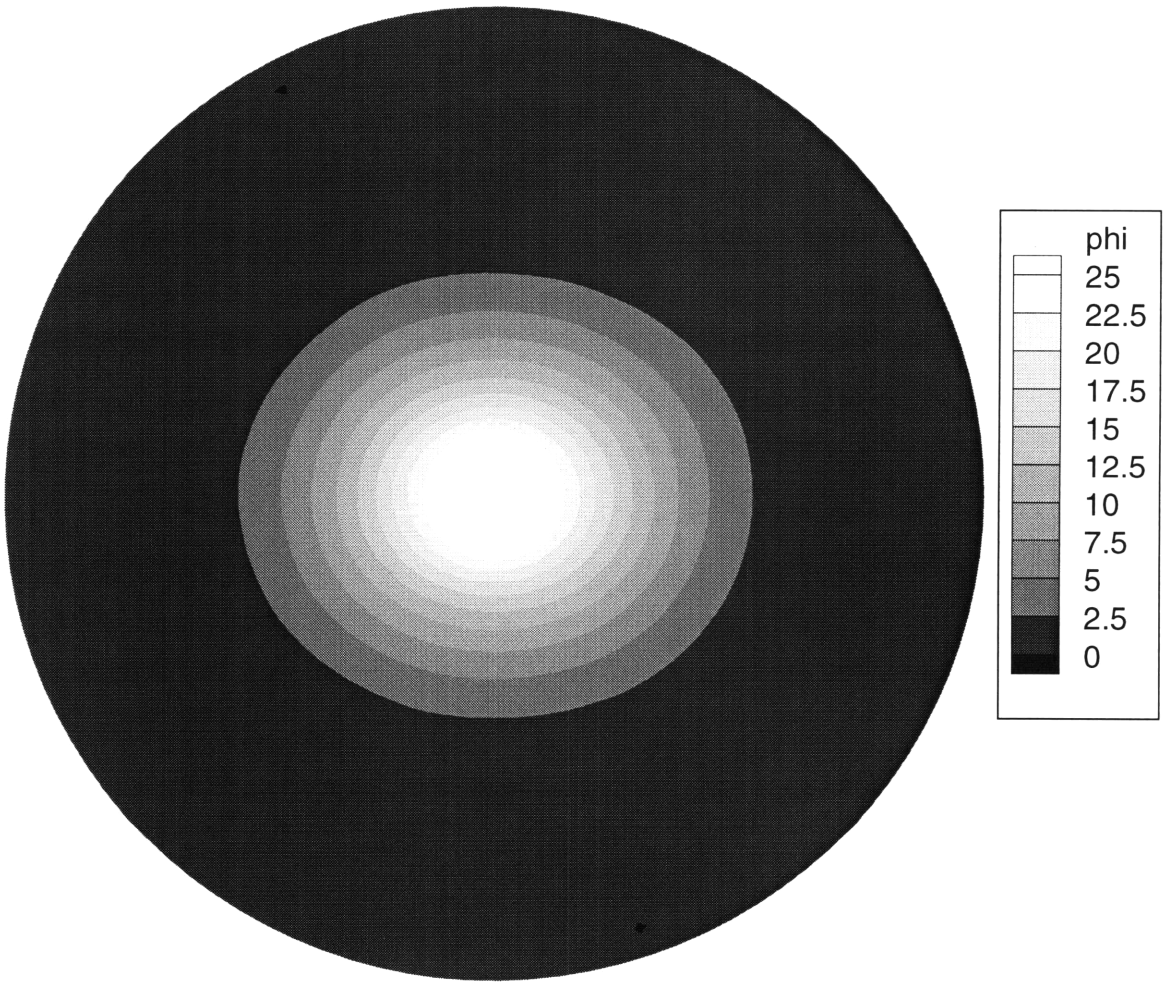

Figure 3-12: Electric potential distribution for the case $\xi_p = 2$

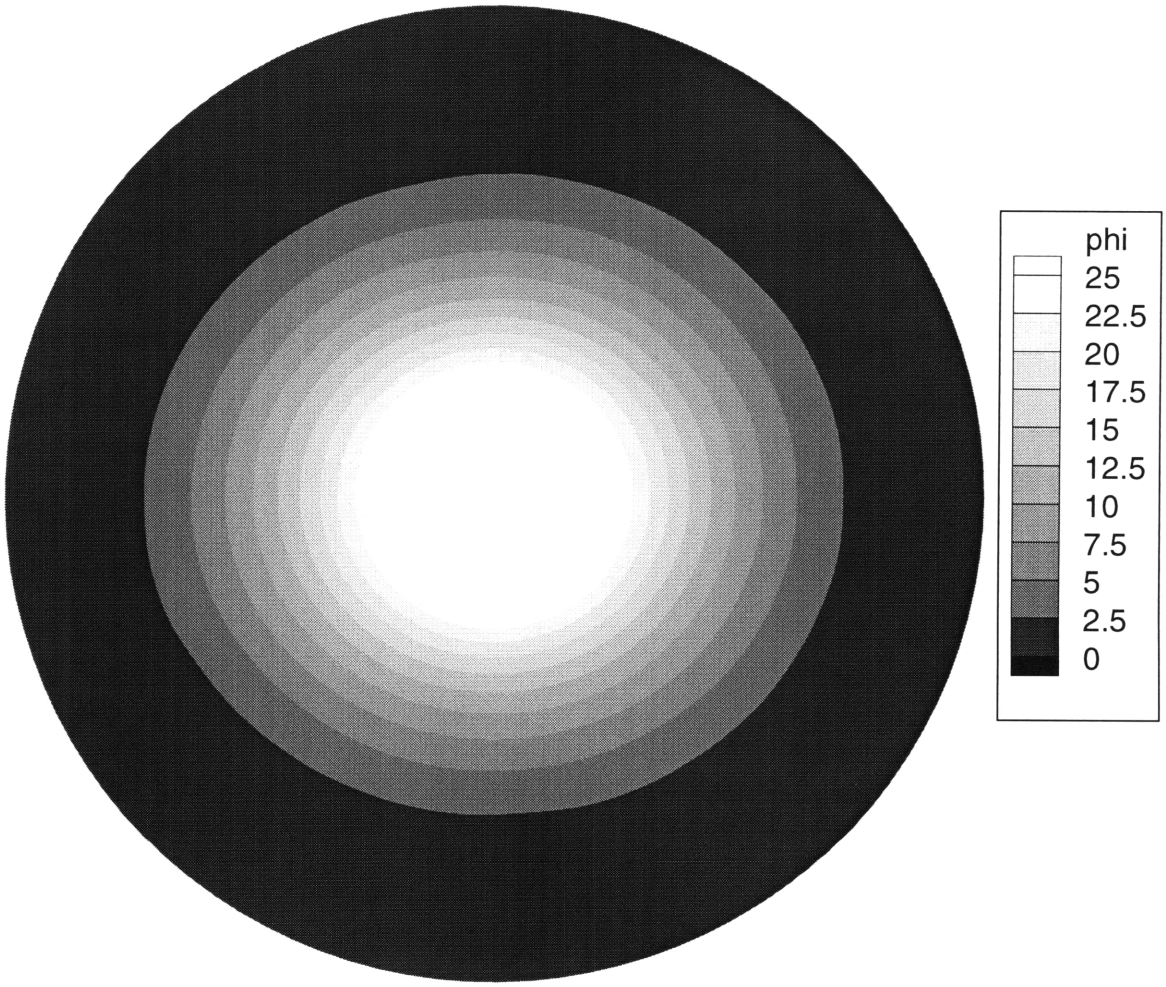

Figure 3-13: Electric potential distribution for the case $\xi_p = 5$

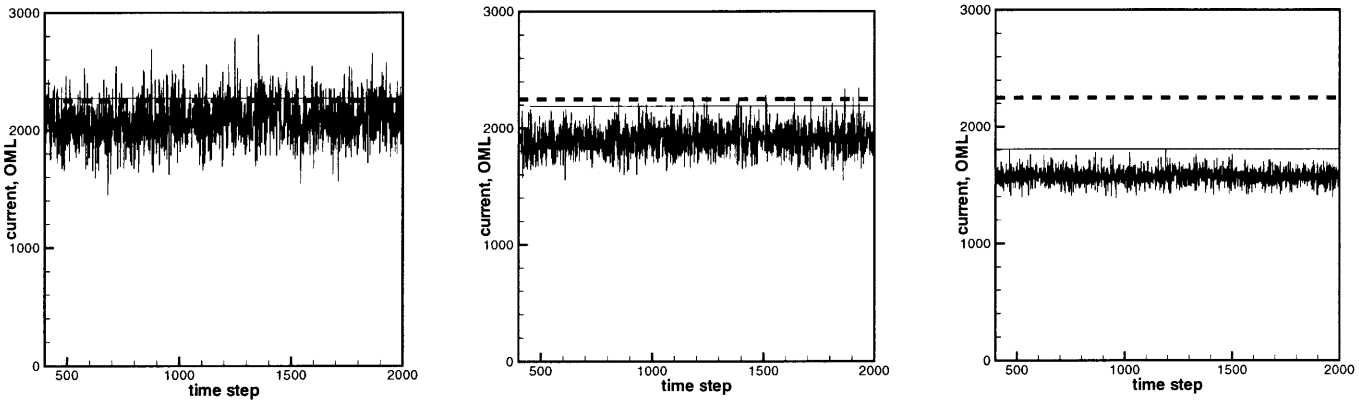

Figure 3-14: History of the Current collection (left) $\xi_p = 1$, (middle) $\xi_p = 2$ and (right) $\xi_p = 5$, the OML current (dashed line) and the exact value (solid line)

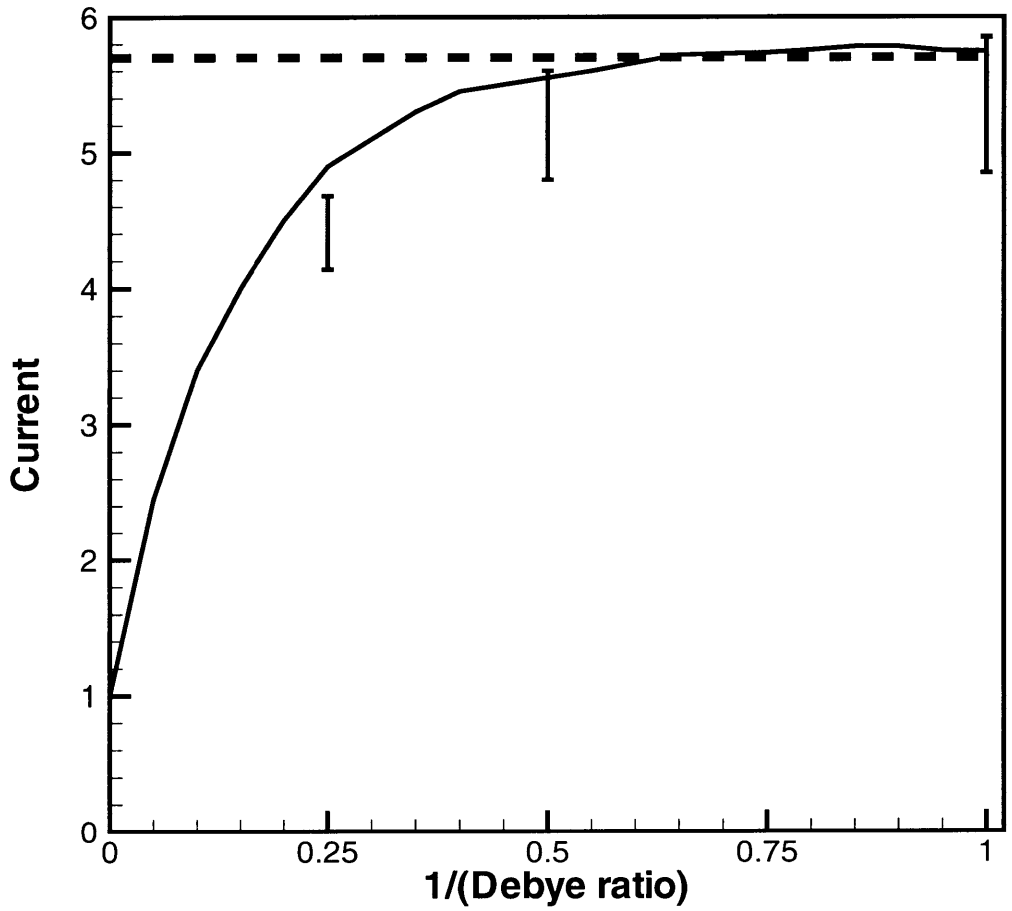

Figure 3-15: Current collection vs. $1/\xi_p$. OML current (dashed), the exact value (solid) and computed value (error bars)

Chapter 4

Conclusion & Further Work

In this chapter, we conclude the possibility and perspective of PIC method to be applied to the space engineering, based on what we discussed in previous chapters. First, we re-state the result from the PIC simulation.

(1) PIC method qualitatively shows the same trend of the current collection with the analytical solution

Figure 3-14 illustrates the exact current collection as a function of the Debye ratio and the value obtained from our simulation. As the Debye ratio decreases, the amount of current collected by the tether gets closer to the limiting value. This limiting value is the one shown by equation (2.13). And as the ratio increase, the current collection decreases. This is because of the bump in the effective potential which prevents the particles from reaching the surface of the tether even if the particle has an enough energy to reach the surface.

(2) PIC method quantitatively shows the current collection with 7% error from the analytical value for all cases of Debye ratio

As illustrated in Figure 3-14, the amount of current collected by the tether oscillates just below the analytical value. The cause of the error can be attributed to the distortion of the grid, as noted before. To avoid this problem, we plan to use different

methods for the interpolation. One possibility is to use the triangular grid with the area-weighting function analogous to one we use in this thesis. The use of the triangular grid does not need the linear interpolation, therefore we can expect to get rid of the error caused by the distortion of the grid.

(3) The current collection code requires non-zero potential as an outside boundary condition.

The partial absorption of electrons requires non-zero potential region, "pre-sheath" outside the sheath. The pre-sheath extends very far. To run the simulation on a relatively small grid, we need to know the local potential at the computational outside boundary. This potential was calculated from the equation of quasi-neutrality. The quasi-neutrality equation relates the local potential to the instantaneous outbound electron density. We calculated the density from the outbound electron flux.

(4) The current collection code can reduce the computational time by using a hypothetically light ion mass.

Since we are only interested in the ion density, not in the ion trajectories, we can use a very light ion mass. The reasonable assumption that no ion is absorbed by the tether allows us to use a very small ion mass. Since the ion density does not depend on the ion mass, when the ions have Maxwellian distribution, the light ion becomes a critical factor to speed up the computation considerably.

Based on this PIC method, we plan to consider (1) the case of flowing unmagnetized plasma, and (2) the case of magnetized plasma as seen in the space engineering application. For either case, the tether potential is still high and, therefore, we can still use the light ion mass. As for the symmetry of the phenomena, we have not taken into account so far any symmetric conditions except for the outside boundary potential, which is taken as an average. This only symmetric condition can be removed by applying local potential values. Therefore, practically this method does not need any symmetry conditions. For future applications, where the symmetry condition is no longer valid, we can apply our PIC method without a substantial modification.

Bibliography

[1] Charles K. Birdsall and A. Bruce Langdon. *Plasma physics via computer simulation.* Institute of Physics Publishing, Bristol and Philadelphia, 1991.

[2] P. M. Chung, L. Talbot, and K. J. Touryan. *Electric Probes in Stationary and Flowing Plasmas; Theory and Application.* SPRINGER-VERLAG, 1975.

[3] H. Goldstein. *Classical Mechanics.* Addison-Wesley Pub. Co., Massachusetts, 1980.

[4] J.G. Laframboise. Theory of spherical and cylindrical langmuir probe in a collisionless, maxwellian plasma at rest. Technical Report 100, University of Toronto Institute of Aerospace Studies Report, 1966.

[5] J.G. Laframboise. Current collection by a positively charged spacecraft: Effects of its presheath. *Journal of geophysical research*, 102(A2), February 1997.

[6] S. Langmuir and H. M. Mott-Smith. The theory of collection in gaseous discharge. *Physical Review*, 28, October 1926.

[7] D. Seldner and T. Westermann. Algorithms for interpolation and localization in irregular 2d meshes. *Journal of Computational Physics*, 79:1–11, 1988.

[8] J. Wang, P. C. Liewer, S. R. Karmesin, and D. Kondrashov. 3-d deformable grid electromagnetic particle-in-cell for parallel computers. *AIAA*, (97-0365), 97.